Supplementary Information

Element mobility and oxygen isotope systematics during submarine alteration of basaltic glass

Miaohong He [1, 2*], Shudi Zhang [3, 4], Le Zhang [1, 2], Fan Yang [1, 2], Yanqiang Zhang [1, 2], Xiaolong Huang [1, 2], Gangjian Wei [1, 2]

[1] State Key Laboratory of Isotope Geochemistry, Guangzhou Institute of Geochemistry, Chinese Academy of Sciences, Guangzhou 510640, China

[2] CAS Center for Excellence in Deep Earth Science, Guangzhou, 510640, China

[3] Department of Public Health and Medical Technology, Xiamen Medical College, Xiamen 361023, Fujian, China

[4] Engineering Research Center of Natural Cosmeceuticals College of Fujian Province, Xiamen Medical College, Xiamen 361023, Fujian, China

1 Major-element analyses by EPMA

The major-element composition of the naturally altered basaltic glass was determined by EPMA, using a JEOL JXA-8100 electron microprobe at the SKLaBIG-CAS, with a 15 kV accelerating voltage, 10 nA current, and 10 μm beam diameter. Counting time was typically 10 s. Standards GSD-1G, BCR-2G, BHVO-2G, and BIR-1G were used for calibration and data-correction purposes. Determination of the major-element composition of the sample involved the same analysis spots as those used for oxygen isotope

determinations, after re-polishing of the sample. Analytical uncertainties were usually better than ±2.5% (1σ).

Supplementary Table 1 Major-element profiles analyses from core to rim of altered glass, (analysis-spot locations as in Fig. 2a) by EMPA. Analytical uncertainties were about ±2.5% (1σ).

location	Na_2O	FeO	K_2O	SiO_2	MnO	CaO	Al_2O_3	TiO_2	P_2O_5	MgO	Total	H_2O
1	3.20	9.94	0.33	51.05	0.16	10.56	14.77	1.87	0.10	7.19	99.18	0.82
2	3.09	9.63	0.36	50.34	0.14	10.61	14.85	1.84	0.13	7.25	98.25	1.75
3	3.06	10.08	0.32	50.94	0.18	10.56	14.87	1.74	0.10	7.22	99.08	0.92
4	3.09	9.97	0.35	51.44	0.20	10.49	14.95	1.72	0.12	7.26	99.60	0.40
5	3.08	9.99	0.37	50.82	0.16	10.58	14.74	1.86	0.14	7.21	98.95	1.06
6	2.95	10.09	0.35	50.88	0.17	10.44	15.10	1.81	0.10	7.30	99.19	0.81
7	2.73	24.29	1.94	43.43	0.03	1.83	10.40	5.67	0.04	2.96	93.30	6.70
8	1.91	17.41	3.11	52.91	0.03	0.96	11.12	2.17	0.01	5.16	94.76	5.24
9	1.58	18.70	3.31	51.74	0.01	0.67	10.50	2.34	0.01	5.11	93.97	6.03
10	1.59	18.21	3.39	51.94	0.08	0.68	10.15	3.00	0.01	5.34	94.39	5.61
Density-corrected values												
1	3.20	9.94	0.33	51.05	0.16	10.56	14.77	1.87	0.10	7.19		
2	3.09	9.63	0.36	50.34	0.14	10.61	14.85	1.84	0.13	7.25		
3	3.06	10.08	0.32	50.94	0.18	10.56	14.87	1.74	0.10	7.22		
4	3.09	9.97	0.35	51.44	0.20	10.49	14.95	1.72	0.12	7.26		
5	3.08	9.99	0.37	50.82	0.16	10.58	14.74	1.86	0.14	7.21		
6	2.95	10.09	0.35	50.88	0.17	10.44	15.10	1.81	0.10	7.30		
7	2.73	24.29	1.94	43.43	0.03	1.83	10.40	5.67	0.04	2.96		
8	1.63	14.89	2.66	45.26	0.02	0.82	9.51	1.86	0.01	4.42		
9	1.35	16.00	2.83	44.26	0.01	0.57	8.99	2.00	0.01	4.37		
10	1.36	15.58	2.90	44.44	0.07	0.58	8.68	2.57	0.01	4.57		

The H_2O contents were calculated based on 100% –total of oxides determined by EPMA. The density-correction perform on palagonite and take basaltic glass as basic, and the calculation was according to the Eq.(3): $c`_{i\,(p)} = (\rho_p/\rho_g) \times c_{i\,(p)}$, The values of ρ_p and ρ_g were determined as 2.56 ($2\sigma = 0.1$) and 2.19 ($2\sigma = 0.1$) $g \cdot cm^{-3}$, respectively.

2 Oxygen isotope and H_2O profiles during palagonitization

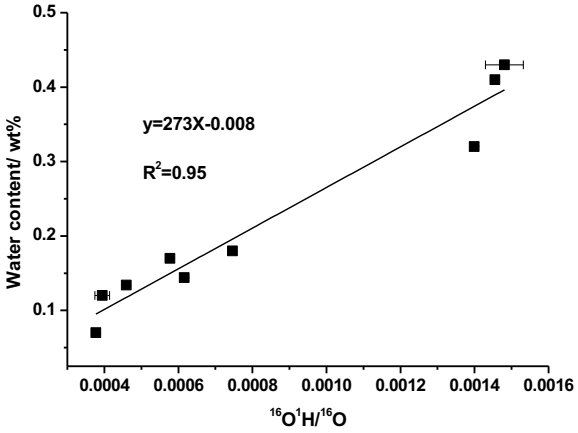

Supplementary Fig. 1 The calibration curve of the ratios of $^{16}O^{1}H/^{16}O$ vs the water content of nine reference materials.

Supplementary Table 2 The water analyses of basaltic glass standards based on SIMS. 1σ is standard deviation.

standards	$^{16}O^{1}H/^{16}O$ by SIMS	1σ /%	N	H_2O content /% [Li, et al, 2019]
G323-9	0.0007461	0.50	3	0.18
G324-10	0.0006157	0.31	3	0.144
G325-11	0.0013994	0.34	3	0.32
G326-12	0.0003944	2.5	3	0.12
G327-13	0.0004594	0.43	3	0.134
G329-15	0.0003772	0.47	3	0.07
G330-16	0.0014807	1.72	3	0.43
G331-17	0.0014551	0.32	3	0.41
ALV-519	0.0005775	0.34	3	0.17

Supplementary Table 3 Oxygen isotopic analyses of basaltic glass standards. Number in parentheses are 1σ standard deviation.

standards	analyses by SIMS			analyses by laser fluorination	IMF/ ‰
	$^{18}O/^{16}O$	1σ/ ‰	N	$\delta^{18}O$/ ‰	
BIR-1G	0.0020292	0.22	15	5.00 (0.02) (Hartley, et al 2012)	6.9
BHVO-2G	0.0020291	0.19	15	5.60 (-) (Hartley, et al 2012)	6.35
GSD-1G	0.0020366	0.24	15	9.64 (0.22) (This study)	6.03
BCR-2G	0.0020295	0.22	15	7.01(-) (Hartley, et al 2012)	5.12

Where IMF= $((^{18}O/^{16}O_{SIMS})/(^{18}O/^{16}O_{V\text{-}SMOW}) - 1) \times 1000 - \delta^{18}O_{laser}$, and $^{18}O/^{16}O_{V\text{-}SMOW} = 0.0020052$.

3 The effect of temperature and pH on precipitation of $Ca(OH)_2$ and $Mg(OH)_2$

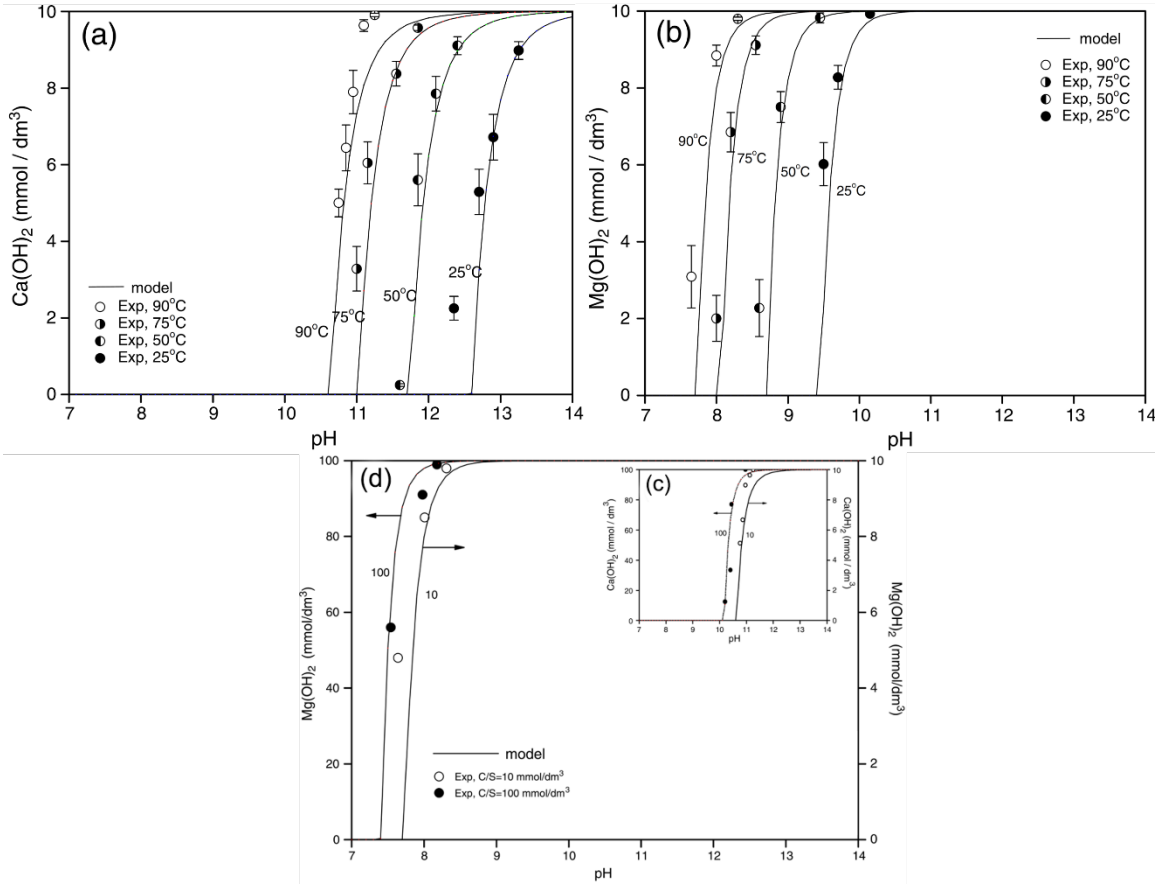

Supplementary Fig. 2 Effect of temperature on precipitation behavior of (a) $Ca(OH)_2$, (b) $Mg(OH)_2$ at different pH value with the initial concentration of Ca^{2+} and Mg^{2+} of 10 mmol/dm^3, which indicates that the precipitation of $Ca(OH)_2$ and $Mg(OH)_2$ would take place at a higher pH by decreasing temperature; (c) and (d) are the effect of initial concentration of Ca^{2+} and Mg^{2+} on precipitation behavior of $Ca(OH)_2$ and $Mg(OH)_2$ at different pH values, respectively, which indicates that the precipitation of $Ca(OH)_2$ and $Mg(OH)_2$ would take place at lower pH with increasing the concentration of Ca^{2+} and Mg^{2+} (T = 90 °C) (Um and Hirato 2014).

4 Trace element distribution patterns

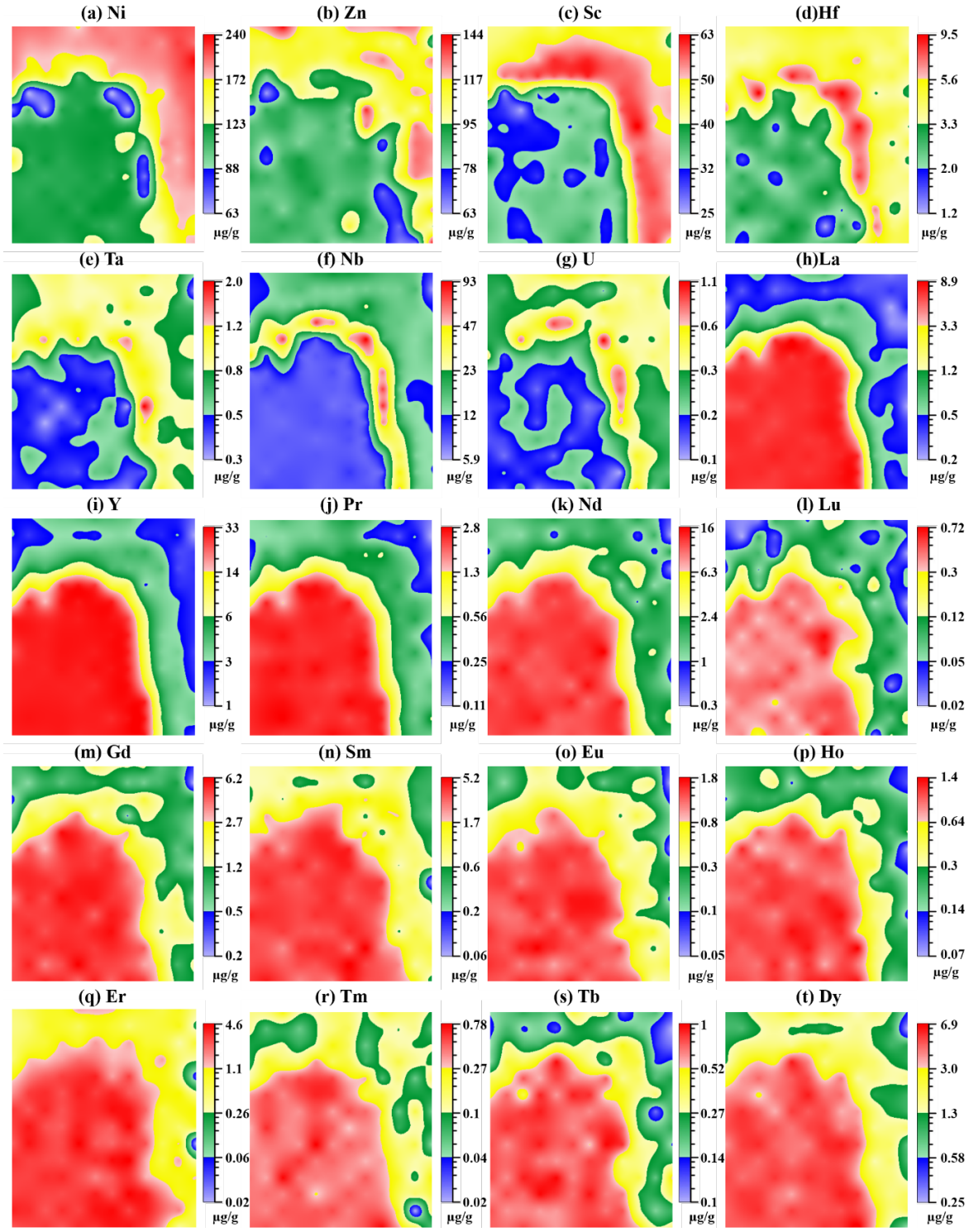

Supplementary Fig. 3 Trace element imaging for (a) Ni, (b) Zn, (c) Sc, (d) Hf, (e) Ta, (f) Nb, (g) U, (h) La, (i) Y, (j) Pr, (k) Nd, (l) Lu, (m) Gd, (n) Sm, (o) Eu, (p) Ho, (q) Er, (r) Tm, (s) Tb, and (t) Dy. Color keys indicate the logarithm of concentration.

5 Scanning electron photomicrographs of the sample

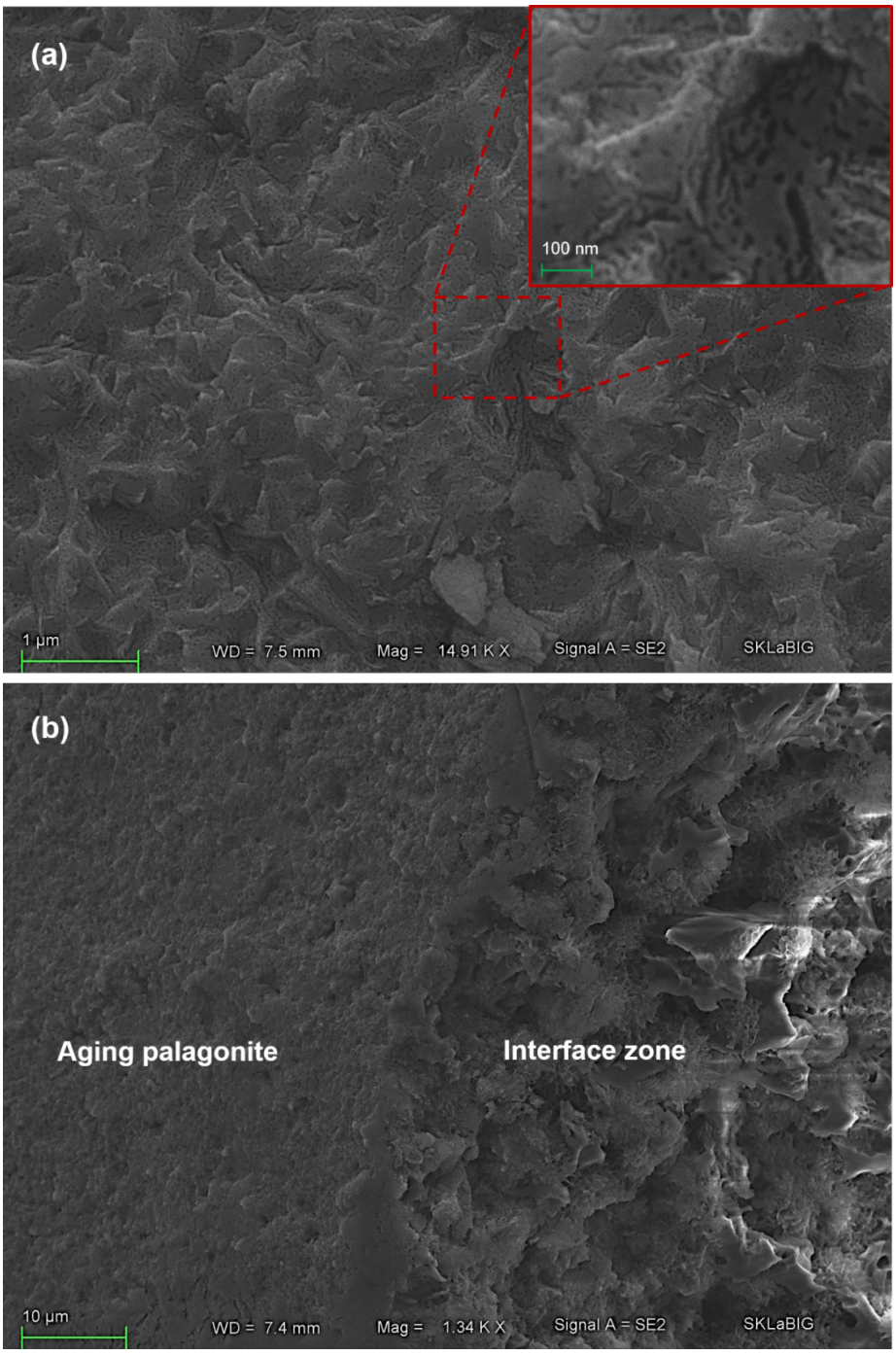

Supplementary Fig. 4 Scanning electron photomicrographs of (a) the aging palagonite, which indicate that there are large amounts of nanometer-sized porosity within palagonite, and (b) the interface zone between basaltic glass and aging palagonite, showing greater porosity and specific surface area than the aging palagonite.

References

Hartley, M. E., Thordarson, T., Taylor, C., Fitton, J. G., and Eimf (2012), Evaluation of the effects of composition on instrumental mass fractionation during SIMS oxygen isotope analyses of glasses, *Chemical Geology*, *334*, 312–323.

Li, Y., Dasgupta, R., and Tsuno, K. (2015), The effects of sulfur, silicon, water, and oxygen fugacity on carbon solubility and partitioning in Fe-rich alloy and silicate melt systems at 3 GPa and 1600 °C: Implications for core–mantle differentiation and degassing of magma oceans and reduced planetary mantles, *Earth and Planetary Science Letters*, *415*, 54-66.

Um, N., Hirato, T., (2014), Precipitation behavior of $Ca(OH)_2$, $Mg(OH)_2$, and $Mn(OH)_2$ from $CaCl_2$, $MgCl_2$, and $MnCl_2$ in NaOH-H_2O solutions and study of lithium recovery from seawater via two-stage precipitation process, *Hydrometallurgy*, *146,* 142-148.